

This work was written as part of one of the author's official duties as an Employee of the United States Government and is therefore a work of the United States Government. In accordance with 17 U.S.C. 105, no copyright protection is available for such works under U.S. Law.

Public Domain Mark 1.0

<https://creativecommons.org/publicdomain/mark/1.0/>

Access to this work was provided by the University of Maryland, Baltimore County (UMBC) ScholarWorks@UMBC digital repository on the Maryland Shared Open Access (MD-SOAR) platform.

Please provide feedback

Please support the ScholarWorks@UMBC repository by emailing scholarworks-group@umbc.edu and telling us what having access to this work means to you and why it's important to you. Thank you.



14 Abstract

15 Measured backscattered UV radiances at 388 ± 1.5 nm are converted to Lambert Equivalent Reflectivity
16 (LER) are from EPIC (Earth Polychromatic Imaging Camera) onboard the DSCOVR spacecraft (Deep Space
17 Climate Observatory) orbiting about the Sun-Earth Lagrange-1 (L_1) gravitational balance point. The
18 average percent of reflected solar energy in the 388 ± 1.5 nm band is 29.2% of the global incident solar
19 energy in that band. Maximum reflected 388 nm solar energy R_{SE} , mostly from clouds, occurs during
20 summer solstice in each hemisphere, December in the Southern Hemisphere SH and June in the
21 Northern Hemisphere NH. The global average R_{SE} (90°S to 90°N) has a maximum in December and a
22 minimum in June showing that the SH cloud reflected energy is greater than that in the NH.
23 Backscattering from land and oceans at 388 nm is small, since the average clear-sky reflectivity of the
24 Earth's surface free of snow and ice is about 0.05. Calculations of R_{SE} based on the 388 nm LER show a
25 7% increase during December 2020 in R_{SE} at 40°S to 50°S when the backscatter angle B_A was 178.05° ,
26 and 6% at 30°S to 40°S in November 2021 when $B_A = 177.5^\circ$ compared to previous years, 2015-2019,
27 with a smaller B_A . Comparison of 380 nm R_{SE} at 40°S to 50°S during December 2020 from the low Earth
28 polar orbiting nadir mapper in the Ozone Mapping and Profiler Suite (OMPS-NM) near 13:30 local solar
29 time suggest that there has been a 5% increase in SH cloud reflection during December 2020 compared
30 to previous years. This suggests that the observed increase by EPIC is mostly from an increase in cloud
31 cover and not from enhanced backscatter. In the NH R_{SE} values at large EPIC B_A (177.5° in June 2020 and
32 178.2° in June 2021) between 30°N to 60°N show a percent decrease 4.8% in R_{SE} at 45°N during June
33 2021 and a 6% increase during June 2020 at 55°N compared to the previous 4 years. This also suggests
34 that the increase and decrease in R_{SE} are probably related to changes in cloud cover and not backscatter
35 angle effects. Annual integrals of percent reflected solar energy over complete years are almost
36 constant at all latitudes.

37

38



39

40 1.0 Introduction

41 The EPIC satellite instrument (Earth Polychromatic Imaging Camera) onboard the DSCOVR (Deep Space
 42 Climate Observatory) observed almost the full illuminated Earth's disk since June 2015 from an orbital
 43 position near the Earth-Sun L_1 point (Lagrange-1 point) approximately 1.5×10^6 km from the Earth. The
 44 spacecraft orbit consists of an approximately 6-month non-repeating tilted Lissajous figure about L_1 that
 45 varies in distance from the Earth ($\pm 1 \times 10^5$ km). The changing orbit causes variations in the instrument's
 46 small satellite viewing angle from the Sun-Earth line (SEV) (Marshak et al., 2021). Recently (2020-2021),
 47 the SEV minimum has decreased from $4^\circ - 6^\circ$ to slightly less than 2° (backscatter angle $B_A = 178^\circ$), which
 48 might cause the observation of reflected radiances to increase compared to observations from smaller
 49 backscattering angles (Marshak et al., 2021, Penttila et al., 2021). The largest enhanced backscatter
 50 effects for small SEV arise in the Near IR (NIR) from vegetation with smaller effects from clouds in the
 51 visible and NIR (Marshak et al., 2021).

52 This paper will examine the cloud-reflected energy in the narrow band 388 ± 1.5 nm where there is
 53 Rayleigh scattering but almost no atmospheric absorption or seasonal dependence of the low surface
 54 reflectivity from land, vegetation, or oceans. Data obtained from two observational platforms will be
 55 compared, one from the EPIC instrument at L_1 and the second from the nadir mapper in the Ozone
 56 Mapping and Profiler Suite (OMPS) onboard the joint NASA/NOAA Suomi National Polar-orbiting
 57 Partnership (Suomi NPP) satellite in an Earth inclined low Earth polar orbit crossing the equator at about
 58 13:30 local solar time. OMPS-NM occasionally observes at large backscattering angles in the equatorial
 59 region but never at higher latitudes.

60 The EPIC instrument observes the Earth in 10 narrow band filter channels from 317.5 nm to 780 nm
 61 (317.5, 325, 340, 388, 443, 551, 680, 688, 764, and 780 nm) using a 30-cm aperture telescope imaging
 62 on a 2048x2048 hafnium coated CCD (Charge Coupled Detector) with a field of view of 0.62° viewing the
 63 Sun illuminated Earth with a nominal angular size of 0.5° . Instrument details and calibration are
 64 discussed in Herman et al. (2018) and Marshak et al. (2018). EPIC obtains between 13 to 22 images per
 65 24 hours depending on the amount of time during a day the receiving antenna at Wallops Island,
 66 Virginia (38° N latitude) is in view of the spacecraft.

67 The OMPS suite of instruments consists of three spectrometers, a spatial nadir mapper OMPS-NM, a
 68 nadir looking ozone profiler, and a limb viewing profiler. Of the three, this paper uses the data from the
 69 downward looking spatial mapper OMPS-NM at 380 ± 0.55 nm. The OMPS-NM side-to-side looking nadir
 70 mapper spectrometer (side-swath of 2000 km) has a spectral range of 300 to 380 nm with a spectral
 71 resolution of 1.1 nm and a nadir spatial resolution of 50×50 km² (Jaross et al., 2012; McPeters et al.,
 72 2019).

73 Unlike the visible and near-IR channels of EPIC, the 380 nm and 388 nm UV reflectivities of clear-sky
 74 snow/ice-free scenes are very low over both land and oceans for both EPIC and OMPS-NM. The average
 75 clear-sky Lambert Equivalent Reflectivity (LER) (Bhartia et al., 1993, Krotkov et al., 1998, 2001; Herman
 76 et al., 2001, Herman et al., 2018) of the snow/ice free Earth's surface is about 0.05 (Herman and



77 Celarier, 1997) after the calculated Rayleigh scattering amount from the surface to the top of the
 78 atmosphere TOA has been subtracted. The observed UV reflectivity is almost independent of seasonal
 79 surface vegetation effects and shadowing effects from the terrain and vegetation and comes mostly
 80 from clouds (Herman et al., 2018).

81 This paper will examine the reflected solar energy R_{SE} in the EPIC narrow band 388 ± 1.5 nm and the
 82 OMPS-NM 380 ± 0.55 nm band. Other than Rayleigh scattering the sources of reflection are from the
 83 clouds, snow/ice, aerosols, land and oceans. The main interest here is the relative year-to-year change
 84 in R_{SE} from 388 ± 1.5 nm or 380 ± 0.55 nm solar irradiance reflected from the illuminated portion of the
 85 Earth as seen by EPIC and OMPS during the period June 2015 to June 2021. This includes the period
 86 (2020-2021) when the minimum EPIC SEV angles were near 2° (B_A near 178°), compared to previous
 87 years 2015-2019 when the minimum SEV angles were larger (4° - 6°). The goal is to see which latitude
 88 bands contribute to the apparent increased back reflection observed by EPIC in June and December
 89 2020 and 2021, and to compare changes in percent reflected energy with SEV angles and the
 90 corresponding measurements from OMPS-NM.

91 The values of reflected energy for OMPS-NM have less point-to-point variation than those for EPIC since
 92 the OMPS-NM is observing mid-day zonal average reflected radiances while EPIC observes spatially
 93 resolved reflected radiances from near sunrise to near sunset. The quantities of interest are the relative
 94 values for each observing instrument during each summer maxima for June and December 2020 and
 95 2021 as a function of latitude compared to the maxima in previous years, 2015-2019.

96 The 1 AU solar flux at 388 nm is approximately $1.04 \text{ W m}^{-2} \text{ nm}^{-1}$ (Thuillier et al., 2003) and at 380 nm is
 97 $1.3 \text{ W m}^{-2} \text{ nm}^{-1}$. The EPIC filter has an almost rectangular Full Width Half Maximum band pass of $\Delta\lambda = 3$
 98 nm (Herman et al., 2018) yielding a solar irradiance at 1 AU at the top of the atmosphere of $E_{TOA} = 3.12$
 99 W m^{-2} . For NPP-NM at 380 ± 0.55 nm, E_{TOA} is 1.43 W m^{-2} . All of the following results will be expressed as a
 100 percent reflected energy incident on the area of a flat disk of radius R_E , $\pi R_E^2 P_{SE}(t, \theta)$ weighted by the
 101 area of each latitude band and the cosine of the solar zenith angle SZA appropriate for the latitude θ ,
 102 longitude, and time t from start of the EPIC ozone data on 17 June 2015 18:44:39 GMT. The EPIC $P_{SE}(t, \theta)$
 103 are corrected for the change in the amount of illuminated Earth seen by EPIC caused by changes in orbit
 104 observing angles during 2021-2022 compared to previous years.

105 **2.0 Reflected Solar Energy R_{SE} and P_{SE}**

106 The intensity of the solar irradiance $F_{SUN}(t)$ at a given Greenwich Mean Time (GMT) on the Earth's
 107 surface is reduced in proportion to the cosine of the solar zenith angle $SZA = \zeta(\theta, \phi, \delta)$, where ϕ =
 108 longitude, θ = latitude, and δ = the Earth's declination angle $-23.45^\circ \leq \delta \leq 23.45^\circ$, Eqs. 1-9. Further
 109 variation is given by the changing Sun-Earth distance caused by the approximately elliptic orbit of the
 110 Earth about the Sun. The illuminated Earth of mean radius $R_E = 6371$ km is divided into latitude by
 111 longitude grids of $0.25^\circ \times 0.25^\circ$. The reflected energy $E_i(\theta_i, t)$ contribution of each latitude band θ_i is
 112 approximately proportional to the illuminated latitude-band area A_i on the Earth (Eqs. 1-5) from M
 113 illuminated grid points. For convenience, the small ($2\Delta\theta = 0.25^\circ$) latitude band contributions can be
 114 summed into 18 ten-degree latitude bands $-90^\circ < \theta < 90^\circ$ using Eq. 6 with the energy reflected in each



band in Watts (Eq. 8), or in percent of R_{SE} appropriate for a given latitude band (Eq. 9). This is followed by a correction for the changing orbit in 2020-2021.

From Eqs. 1-9, the EPIC sunrise to sunset 388 ± 1.5 nm reflected energy ($90^\circ S$ to $90^\circ N$) from clouds, aerosols, the surface, and snow/ice is $P_{SE} = 29.2\%$ of the incident solar energy including the surface contribution. Annual integrals of reflected energy are almost constant.

For OMPS-NM, the spatial grid is $\Delta\theta = 0.5^\circ$ and $\Delta\phi = 0.5^\circ$ corresponding to its coarser spatial resolution and the summation in Eq. 5 is over 360° since OMPS-NM makes 1 measurement per 24 hours for a given grid point at fixed solar time near 13:30 local solar time. $N = 40$ for EPIC in Eq. 7 and 20 for OMPS-NM.

$$A_i(\theta_i, \phi, \Delta\theta) = 2\pi R_E^2 [\sin(\theta_i + \Delta\theta) - \sin(\theta_i - \Delta\theta)] \frac{\Delta\phi}{2\pi} \quad (1)$$

$$A_i(\theta_i, \phi, \Delta\theta) = R_E^2 B_i(\theta_i, \Delta\theta) \Delta\phi = \text{Area of one grid box} \quad (2)$$

$$\text{where } B_i(\theta_i, \Delta\theta) = 2 \cos(\theta_i) \sin(\Delta\theta) \quad (3)$$

$$\text{and } \Delta\phi = 0.25\pi/180 \text{ and } \Delta\theta = 0.125\pi/180 \quad (4)$$

$$E_i(\theta_i, t) = R_E^2 F_{\text{Sun}}(t) \sum_{j=1}^M [\cos(\zeta(\theta_i, \phi_j, t)) L_{ER}(\theta_i, \phi_j, t)] B(\theta_i, \Delta\theta) \Delta\phi \quad (5)$$

$$E_i(\theta_i, t) = R_E^2 F_{\text{Sun}}(t, \Delta\lambda) G_i(\theta_i, t) \quad (\text{Watts}) \quad (6)$$

$$G_k(\theta_k, \Delta\theta) = \sum_{j=1}^N G_{j,k}(\theta_{j,k}) \text{ for } k = 1, 18 \text{ for the band width } \Delta\theta = \frac{\pi}{18} \quad (7)$$

$$I(t, \theta_k, \Delta\theta) = F_{\text{Sun}}(t, \Delta\lambda) R_E^2 G_k(\theta_k, \Delta\theta) \quad (\text{Watts}) \quad (8)$$

$$P_{SE}(t, \theta_k, \Delta\theta) = 100 \frac{G_k(\theta_k, \Delta\theta)}{\pi} \quad (\text{Percent}) \quad (9)$$

The global percent reflected energy P_{SE} appears to increase in the SH during December 2020 ($SEV = 1.95^\circ$) (Table 1) compared to previous years (2015-2019) when the SEV angles are larger. Part of the 2020 - 2021 increase may be caused by enhanced backscatter (Marshak et al., 2021) from clouds and part from the Earth's surface. There are also small SEV angles in June 2021 that corresponds to the maximum reflected energy in the NH that do not show and enhanced P_{SE} . Sections 2.1 and 2.2 will show which latitude bands contribute to the global ($90^\circ S$ to $90^\circ N$) increased reflected energy during 2020 – 2021 shown in Fig. 1.

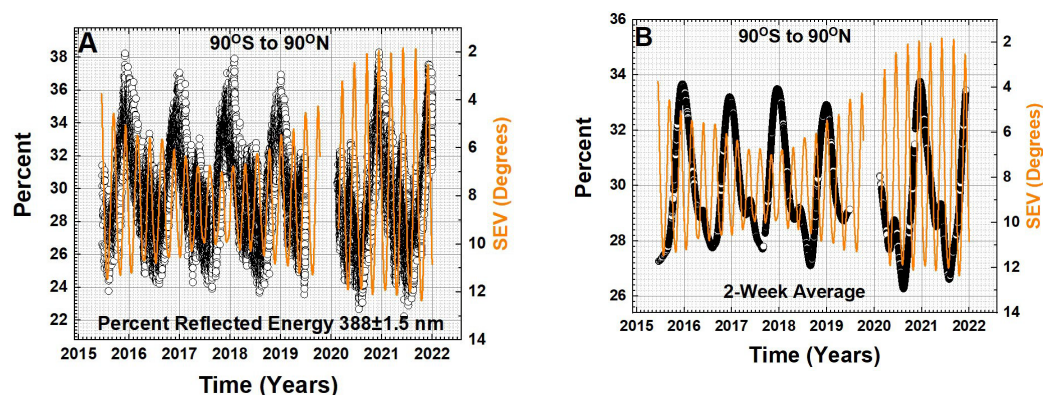


Fig.1 Panel A: Percent reflected solar energy P_{SE} for the Earth from 90°S to 90°N in the narrow band 388±1.5 nm (black circles one for each EPIC scene) from clouds, aerosols, and surface as a function of time and SEV angle (orange curve – right axis). There are about 6000 points per year. Panel B: 2-week running average to more clearly show the December and June peaks.

131

132

Table 1 Minimum SEV angles

133

Date	SEV (Deg)
19 March 2020	3.25
16 June 2020	2.46
15 September 2020	2.10
11 December 2020	1.95
7 March 2021	2.05
3 June 2021	1.83
2 September 2021	1.88
29 November 2021	2.53

136

137

138

139 Most of the apparent scatter of data points for EPIC in Fig. 1 is not measurement noise but instead is the
 140 result of obtaining multiple measurements of the rotating Earth every day. Figure 2 contains a small
 141 subset of data points obtained from 20 March 2016 to 30 March 2016 showing the successive maxima
 142 occurring over the Pacific Ocean and the minima over Africa. This is opposite of the behavior for the
 143 visible and NIR channels that have much higher surface reflectivity, especially over Africa and over
 144 vegetation. Since the data are from March, the NH winter cadence applies for 13 points per 24 hours
 145 compared to the NH summer cadence of 21 points per 24 hours. The same interpretation of apparent
 146 scatter in EPIC data points applies to every figure. The summer/winter difference in cadence is caused
 147 by the location of the data receiving antenna at Wallops Island, Virginia (37.9°N) changing the number
 148 of hours the spacecraft is in view.

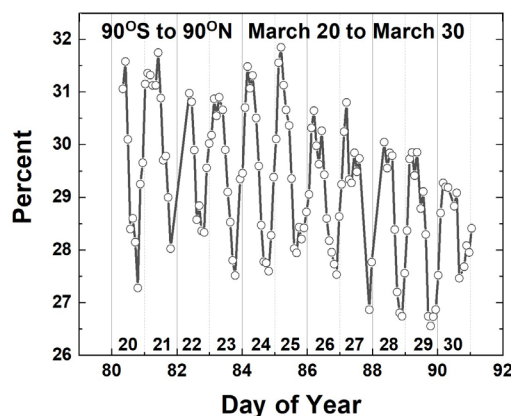


Fig. 2 EPIC's daily variation of $P(t)$ caused by the Earth's rotation for $\Delta\theta = 90^\circ\text{S}$ to 90°N from 20 March 2016 to 30 March 2016 corresponding to the grey circles in Figure 1A. The numbers 20 to 30 represent the dates in March 2016.

149

150 2.1 Southern Hemisphere

151 The maximum percent reflected energy P_{SE} in each hemisphere occurs during their respective summer
 152 months corresponding to the minimum SZA at a given latitude caused by the varying solar declination
 153 angle $\pm 23.45^\circ$ during the earth's annual orbit about the sun. In the SH there is a clear P_{SE} increase (Fig.3)
 154 in December 2020 ($SEV=1.95^\circ$) for latitudes greater than 30° compared to previous years. A smaller
 155 increase in P_{SE} occurs at the end of November 2021 ($SEV = 2.53^\circ$). In the NH there are also
 156 correspondences of the summer P_{SE} maxima with minimum SEV angle (1.83°) in June 2021 and June
 157 2020 (2.46°). As shown later, NH P_{SE} values do not show an increase compared to previous years.

158 The SH quantity of interest is the peak during December 2020 when the SEV angle was about 1.95°
 159 compared to the average peak of the preceding years when the SEV angle was 6° to 7° (Figs. 1 and 3).
 160 Because of the small SEV angle, EPIC observes more of the illuminated disk at $SEV=2^\circ$ than at $SEV=6^\circ$.
 161 The missing area near the Earth's limb rotates east and west and north and south with the satellite orbit.
 162 The worst case for mid-latitudes is when the orbit is aligned with the latitude of interest. After cosine
 163 weighting for reflected energy from the Earth's edges, there is an increase in observed reflected energy
 164 at mid-latitudes when the SEV angle is 2° compared to 6° from just the observing geometry.

165 Figure 3 shows ratio of observed cosine weighted illuminated areas as a function of month of the year
 166 for four SH latitude bands as observed by EPIC during 2020-2021 with $SEV \approx 2^\circ$ to that during the years
 167 2015-2019 when SEV was 4° - 6° . The ratios of the observed areas in December, $A_c = \text{Area in 2020}/\langle \text{Area}$
 168 $2015-2019 \rangle$, are 1.03 for 35°S , 55°S , and 65°S , and 1.04 for 45°S , where $\langle \dots \rangle$ denotes average. To
 169 compare the reflected energy from 2015-2019 to that from 2020 Eqs. 8 and 9 for 2020 must be divided
 170 by A_c . for this purpose, the smoothed Loess(2-months) data are used (Cleveland, 1981). The results are
 171 shown in Fig.4 for four latitude bands.

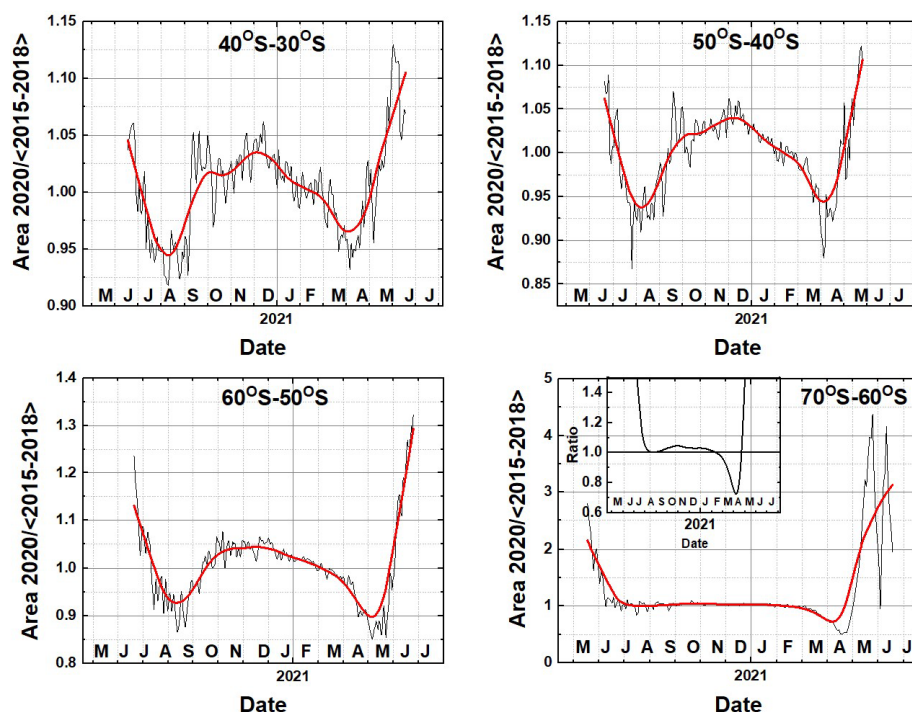


Fig. 3 The ratio $R_A = A(2020)/\langle A(2015-2018) \rangle$ of the Earth's area within the specified latitude bands seen by EPIC in 2020 to that seen during the years 2015-2019. In December 2020, the ratio is 1.03 for 35°S, 55°S, and 65°S, and 1.04 for 45°S. The red curve is Loess(2-months). The inset in 70°S-60°S shows the details near December 2020.

172

173 Figure 4 shows SH EPIC percent reflected energy $P_{SE}(388 \pm 1.5 \text{ nm})$ for six 10° wide latitude bands
 174 compared to the SEV angles with $R_A = A(2020)/\langle A(2015-2018) \rangle$ applied. The dates of the minimum SEV
 175 angles are shown in Table 1 with a clear minimum SEV angle match on 11 December 2020 and 29
 176 November 2021 (Fig. 3 and Appendix Fig. 1A), except at latitudes poleward from 70°S where the peak
 177 P_{SE} occurs just after the SEV minimum. At mid-latitudes, 30°S to 70°S the SEV December minimum and
 178 the P_{SE} maximum match closely. For lower latitudes 0–20, the P_{SE} peaks do not show and increase and
 179 are significantly wider.

180 The approximate equivalent of a seven-day least-squares running average (Cleveland, 1981), Loess(f),
 181 where f= fraction of data points in the entire time series, is performed on the data set corresponding to
 182 approximately 13 illuminated Earth views per 24 hours in December using Loess(0.035). For the 7 days
 183 surrounding the minimum SEV=1.96° on 10 December the range of SEV angles that are included in the
 184 averaged P_{SE} spans 1.96° to 2.43°. The specific day of the December peak P_{SE} varies with latitude so that
 185 it occurs slightly after the 10 December minimum SEV at latitudes 90°S to 70°S but closely matches the
 186 minimum SEV time for latitudes 70°S to 10°S with lower latitudes 10°S to 40°S having a wider peak (Fig.
 187 4).



9

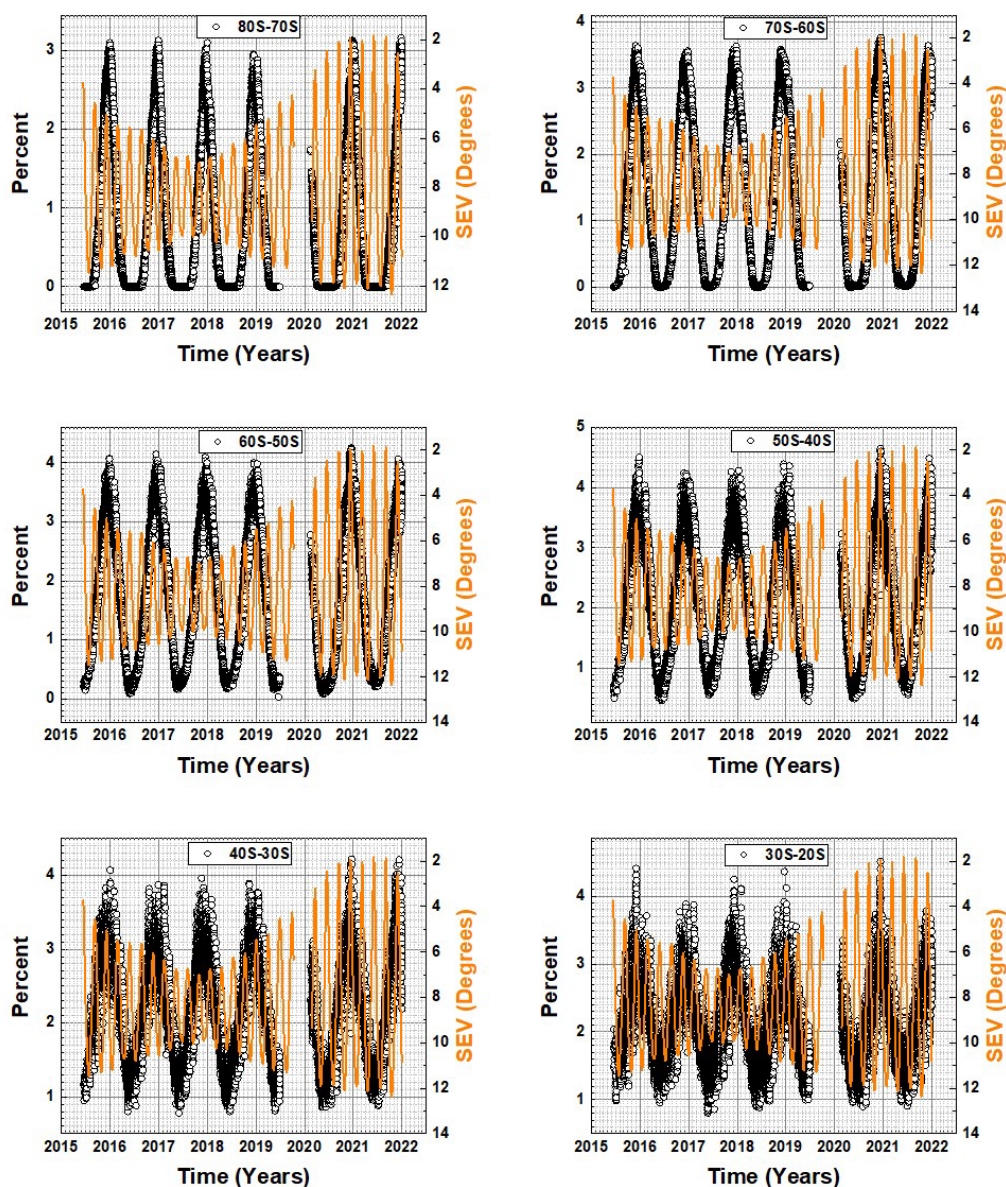


Fig. 4 EPIC SH percent reflected solar energy in the $P_{SE}(388\pm1.5\text{ nm})$ band (grey circles), the SEV angles (orange). Magnified details are shown in the Appendix Fig. A1.

188

189 An alternate graph comparing different years is shown in monthly average P_{SE} (Fig. 5) for the SH showing
 190 that the largest effect is in the 40°S to 50°S latitude band centered in December 2020 (orange curve).

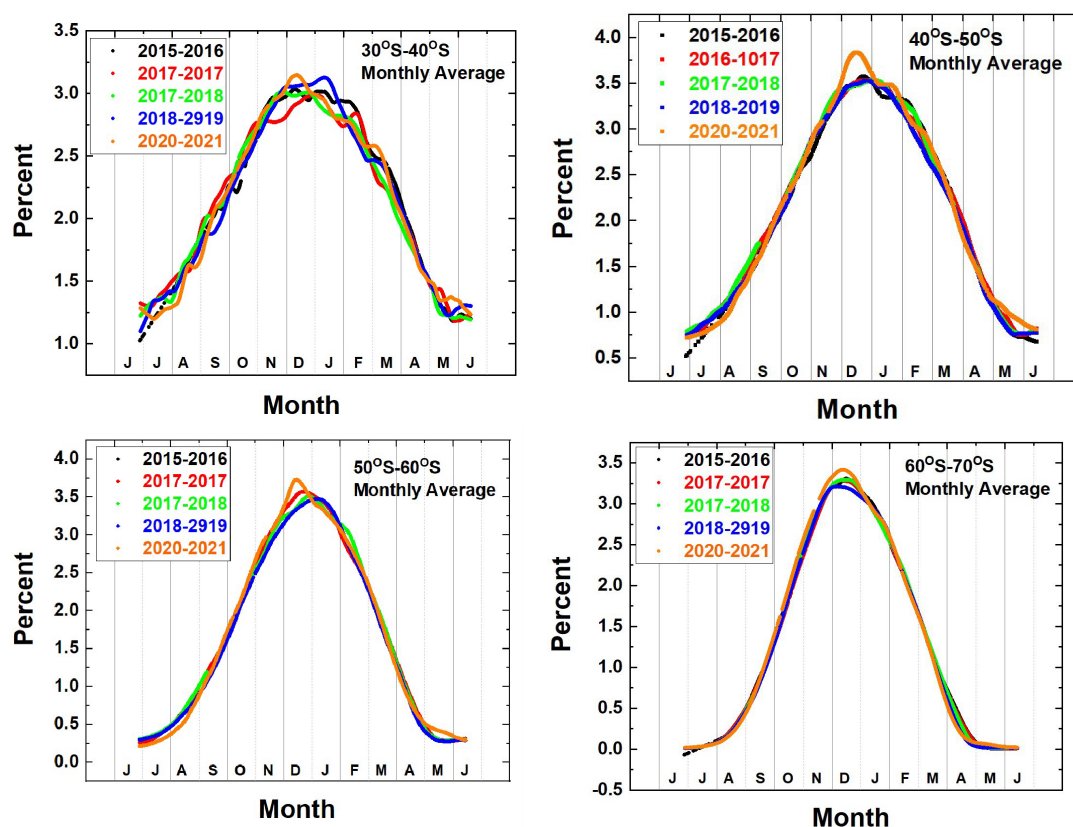


Fig. 5 Monthly average of SH annual time series of percent reflected energy at 388 ± 1.5 nm for 5 years, 2015 – 2021 for 4 latitude bands.

191

192 The results of Figs. 4 and 5 are summarized in Fig. 6 as a function of latitude showing comparisons of the
 193 P_{SE} peak values in December 2020 and November 2021 compared to previous years. The maximum P_{SE} is
 194 at 45°S during December 2020 (4.19%, orange curve) compared to the 4-year average (3.77%). Similar
 195 data from November 2021 shows almost no difference (3.89%) compared to the 4-year average (3.77%).



11

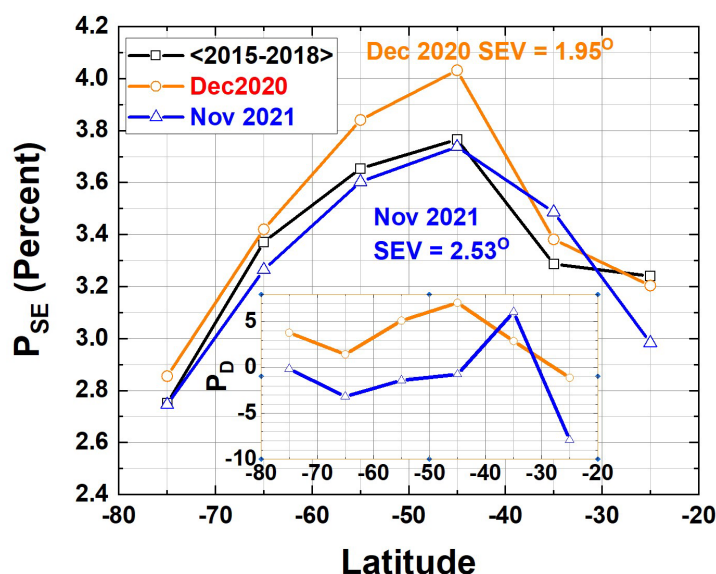


Fig. 6 One-week least squares running averages Loess(0.035) of P_{SE} values from Fig. 3 as a function of latitude for the periods Dec 2020 ($SEV = 1.95^\circ$) and November 2021 ($SEV = 2.53^\circ$) compared to the average of the preceding 4 years, 2015-2018 ($4^\circ < SEV < 6^\circ$). The symbols <A-B> denote average. The inset shows the percent difference P_D as defined in Eq. 10.

$$P_D = 100 \left(\frac{P_{SE}^Y - P_{SE}^{Avg}}{P_{SE}^{Avg}} \right) \quad Y = 2020 \text{ or } 2021 \quad (10)$$

196

197

198 Figure 7 shows the EPIC-view hemispheric zonal average for OMPS-NM for the latitude band $50^\circ S$ - $40^\circ S$
 199 compared to 1 to 2 hour time-dependent P_{SE} from EPIC. The peak values for the December solstice
 200 maxima are in close agreement while the June solstice minima do not agree $P_{SE}(EPIC, \text{June}) < P_{SE}(OMPS,$
 201 $\text{June})$ since $P_{SE}(OMPS, \text{June})$ are computed from a zonal average that always includes more clouds than
 202 the minimum values of $P_{SE}(EPIC, \text{June})$ occurring over Africa (Fig. 2).

203 The EPIC SH cloud peak reflected energy aligns with the small SEV angle (1.96°) in December 2020 and
 204 the percent difference P_D (Eq. 10) is $P_D = 5.4\%$ compared to the preceding 4 years. The OMPS-NM
 205 December 2020 peak also exceeds the average of the preceding 5 years by $P_D = 5\%$. This suggests that
 206 the increase in December 2020 is from increased cloud cover and not from enhanced backscatter when
 207 $SEV = 1.96^\circ$.

208

209

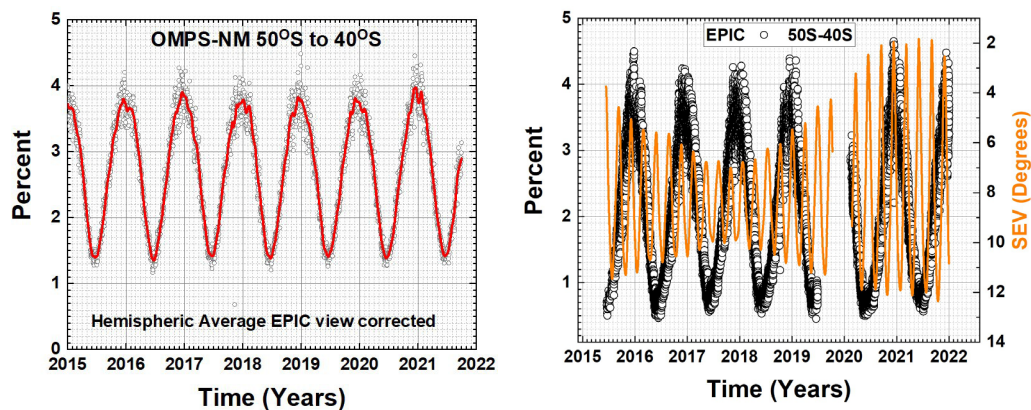


Fig. 7. A time series of OMPS-NM hemispheric zonal average P_{SE} (1 point per day grey circles) 2015–2021.5 and a 1-week average (red curve) for the band 40°S to 50°S compared to EPIC P_{SE} . The red-curve is a 1-week running average Loess(0.028).

210

Table 2 Summer Solstice Area Ratios (Figs 3 and 8)
 $R_A = A(2020)/\langle A(2015-2018) \rangle$

Latitude	R_A	Latitude	R_A
65S	1.03	65N	0.97
55S	1.03	55N	0.97
45S	1.04	45N	0.99
35S	1.03	35N	0.99
25S	1.04	25N	1.00
15S	1.02	15N	0.95
5S	1.02	5N	1.01

211

212 **2.2 Northern Hemisphere**

213 The NH June peaks in P_{SE} coincide with the SEV minima of 16 June 2020 (2.46°) or 3 June 2021 (1.83°) in
214 5 of the 6 latitude bands shown (Fig. 8). Exceptions are for 0 to 10°N, 10°N to 20°N, and 20°N to 30°N.
215 For the latitude bands where there is coincidence between the maxima in $P(t, \theta, 10)$ and minima SEV one
216 might expect enhanced backscattering corresponding to the June minimum SEV compared to previous
217 years as there is in the SH. However, this is not the case (Figs. 8, 9, 10).

218

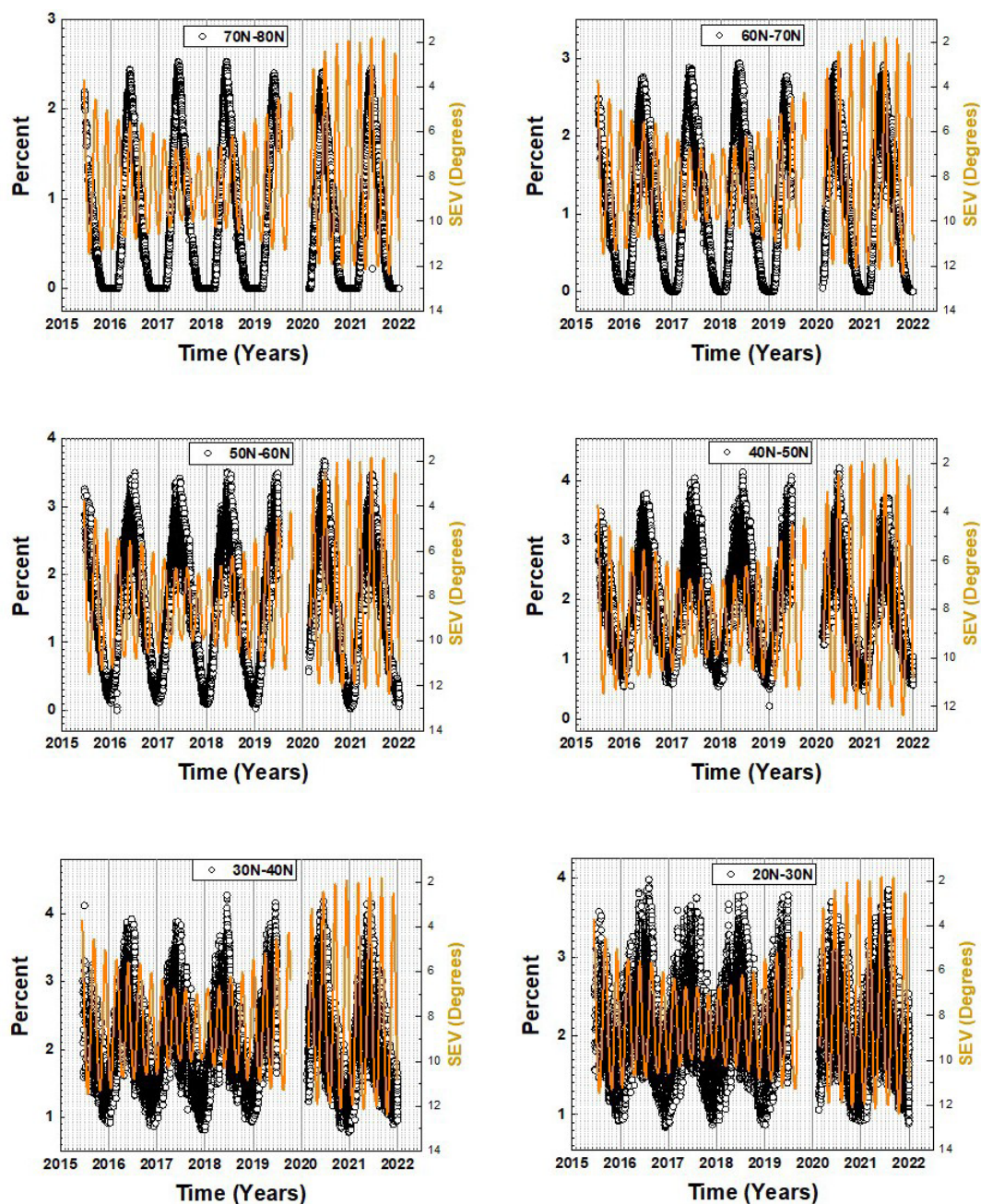


Fig. 8 EPIC NH percent reflected solar energy in the $P_{SE}(388\pm1.5\text{ nm})$ band (grey circles), the SEV angles (orange). Magnified details are shown in the Appendix Fig. A1.

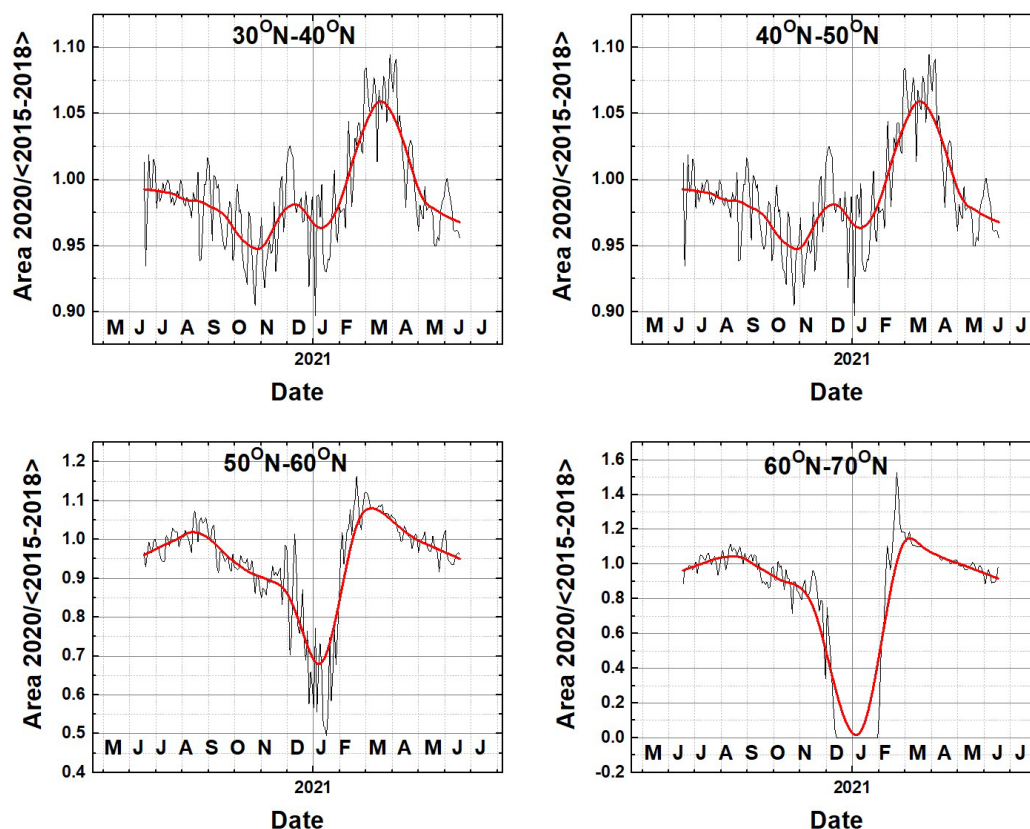


Fig. 9 The ratio $R_A = A(2020)/\langle A(2015-2018) \rangle$ of the Earth's area within the specified latitude bands seen by EPIC in 2020 to that seen during the years 2015-2019. In June 2020, the ratio is 0.96 for 35°N, 0.96 for 45°N, 0.97 for 55°N, 0.93 for 65°N. The red curve is Loess(2-months).

220

221 Because the DSCOVR orbit about L_1 has an approximately six-month period superimposed on a longer
 222 period of about 5 years when the orbit shape changes from an ellipse to a circle and back to an ellipse,
 223 the observed area effect in the NH was different than in the SH when the SEV angles became small. The
 224 June solstice area ratio values are closer to 1.

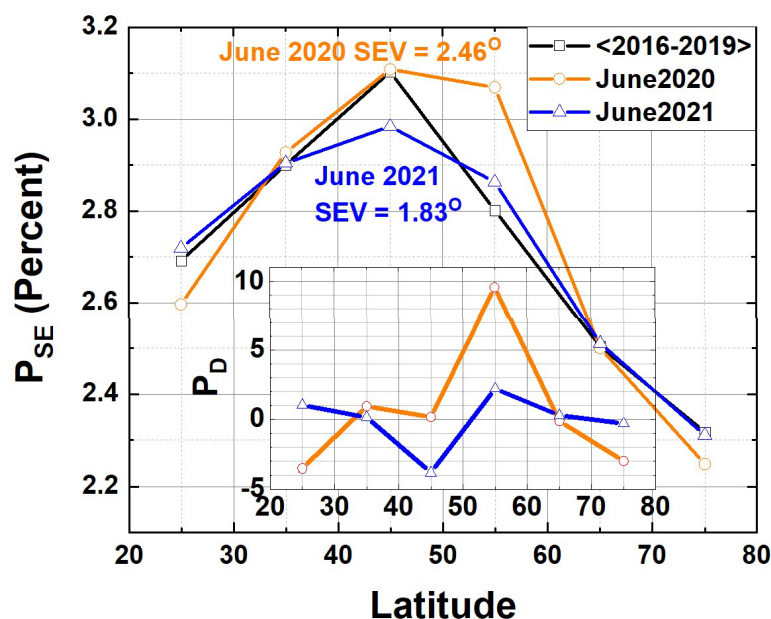


Fig. 10 Peak 1-week least squares running averages Loess(0.006) of P_{SE} values from Fig. 8 as a function of latitude for the periods June 2020 ($SEV = 2.46^\circ$) and June 2021 ($SEV = 1.83^\circ$) compared to the average of the preceding 4 years, 2016-2019 ($4^\circ < SEV < 6^\circ$). The symbols <A-B> denote average. Inset is Percent Difference P_D vs Latitude as in Eq. 10.

228

229 The June 2021 peak P_{SE} data ($SEV = 1.83^\circ$) shows a decrease ($P_D = -4.8\%$) at ($40^\circ N - 50^\circ N$) relative to the
 230 preceding 4 years (2016-2019) suggesting that there was no significant backscatter effect and that the
 231 cloud amount decreased. The period June 2020 ($SEV = 2.46^\circ$) shows no significant change at $45^\circ N$ and
 232 an increase at $55^\circ N$ of $P_D = 9\%$, which is probably due to increased cloud amount since the SEV angle is
 233 2.46° . The NH time monthly average time series for each year (Fig. 11) can be compared in a manner
 234 similar to Fig. 4 showing that the small SEV period during 2021 (blue curve) does not show an enhanced
 235 backscatter effect, but instead a decrease in reflected energy compared to <2016-2019>.

236

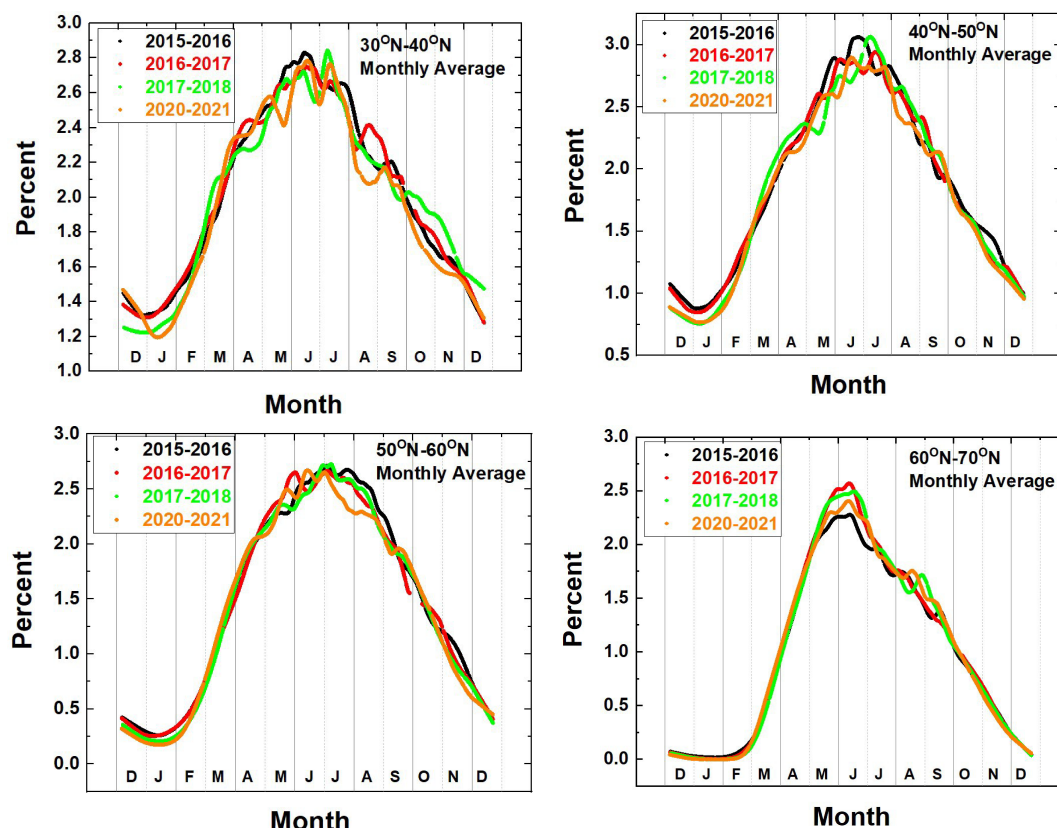


Fig. 11 Monthly average of NH annual time series of percent reflected energy at 388 ± 1.5 nm for 4 years, 2015 – 2021.

237

238 3.0 Summary

239 EPIC observed 388 ± 1.5 nm backscattered irradiances are mostly from clouds since the average 388 nm
 240 reflectivity of the Earth's snow/ice-free surface is small, approximately 0.05. At all non-equatorial
 241 latitudes, the maximum reflected energy occurs during the summer solstice (minimum SZA). During the
 242 period 2020 to 2021, the backscatter angle became close to 178° in December 2020 compared to 174° –
 243 176° in prior years (2015 – 2019), which might lead to enhanced reflected energy. The analysis of
 244 showed that there was a significant increase in reflected energy, $P_D = 7\%$, in the latitude band 40°S –
 245 50°S during December 2020 with smaller effects at other SH latitudes $P_D = 3\%$ at 35°S and 5% at 55°S
 246 and none near the equator. If the increases were due to enhanced backscatter, one would have
 247 expected the same enhanced backscatter in the NH during June 2021 from P_{SE} peaks that coincide with
 248 the SEV minimum ($SEV = 1.83^\circ$). Instead, there was a decrease at 45°N and almost no increase at 55°N .
 249 The $P_D = 8\%$ increase at 55°N ($SEV = 2.46^\circ$) shown in Fig. 11 suggests that the increase was from change
 250 in cloud cover in the NH with backscatter effects being small. Comparison with the polar orbiting OMP-
 251 NM (SEV greater than $40^\circ - 23.45^\circ = 16.55^\circ$) percent reflected energy at 380 ± 0.55 nm showed a 5%



252 December 2020 increase at $45^{\circ} \pm 5^{\circ} \text{S}$ implying there was an increase in cloud cover seen by both EPIC
253 and OMPS-NM. However, the global annual integral of reflected $388 \pm 1.5 \text{ nm}$ energy is almost constant.

254 Two recent papers, Marshak et al., (2021) and Penttilä et al. (2021) suggested that the increase in
255 observed reflected sunlight might be from enhanced backscattering in the SH when the SEV angle was
256 close to 2° . The increase seen by Marshak et al., was mostly from land surfaces in the visible wavelength
257 ranges. The analysis of Penttilä et al. (2021) suggested that about half might be caused by increased
258 cloud cover. The results of the current analysis (EPIC observed increase of $P_D = 7\%$ at 45°S and 5% at
259 55°S and 5% observed from OMI-NM at 45°S) suggest that most of the increase in reflected energy in
260 December 2020 comes from an increase in cloud amount.

261



262 4.0 Appendix

263 Figure A1 shows magnified details for 2 latitude bands each in the NH and SH along with the coinciding
 264 minimum SEV data.

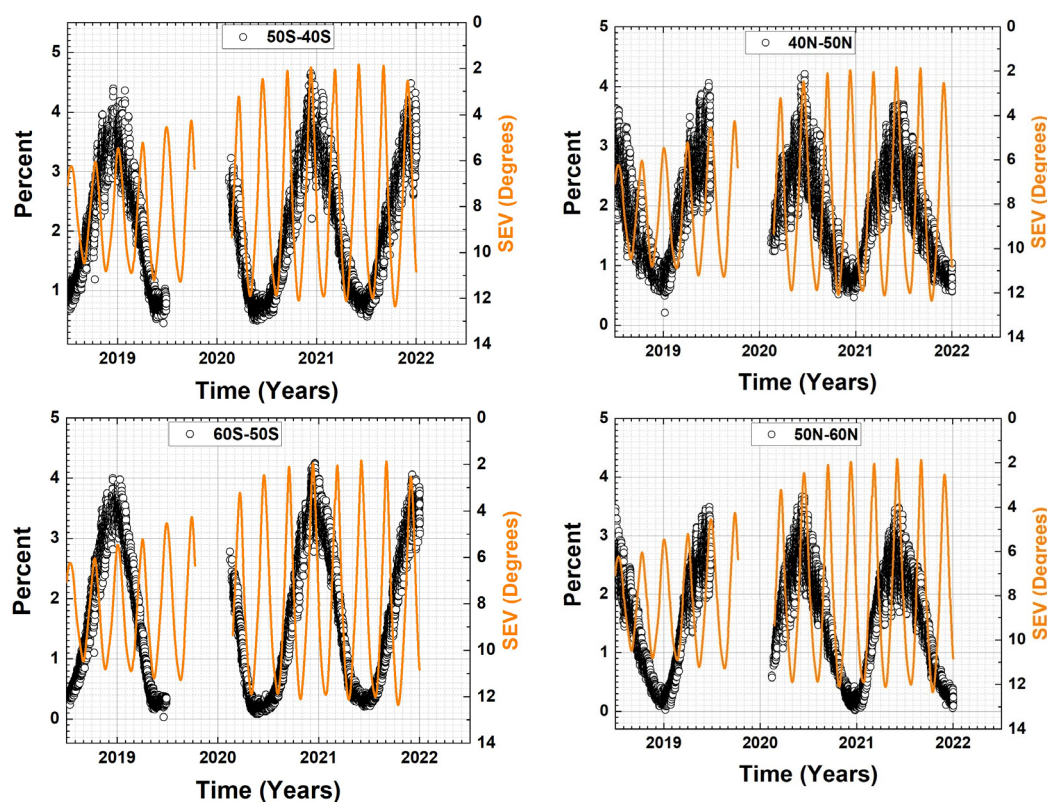


Fig. A1 Magnified samples from Figs. 3 and 7 showing SEV minimum coincidences with P_{SE} maxima in the SH and NH. The SEV are colored orange.

265

266



267 **Author contribution:**

268 Jay Herman is responsible for writing the text, calculations in the paper, and all the figures. Liang-
269 Kang Huang is responsible for supplying the available EPIC LER data as a function of latitude,
270 longitude and time. He also suggested many technical improvements. Dave Hafner also helped
271 supply the LER data and the OMPS-NM data. Adam Szabo suggested the original idea for the paper.

272 **Data Availability**

273 The data used are publicly available in an Excel and Zip format at Open Science Framework

274 <https://osf.io/r3xpt/>

275

276 **Competing interests:**

277 The authors declare that they have no conflict of interest.

278 **Acknowledgements:**

279 The authors want to acknowledge the contribution and help of the EPIC science team and support
280 from the Project team in making the EPIC data freely available.

281



5.0 References

- Bhartia, P. K., J. Herman, R. D. McPeters, and O. Torres, Effect of Mount Pinatubo aerosols on total ozone measurements from backscatter ultraviolet (BUV) experiments, *J. Geophys. Res.*, 98, 18,547-18,554, <https://doi.org/10.1029/93JD01739>, 1993.
- Cleveland, William S., *LOESS: A program for smoothing scatterplots by robust locally weighted regression. Am Stat.* 35 (1): 54. [JSTOR 2683591](https://www.jstor.org/stable/2683591). doi:10.2307/2683591, 1981.
- Herman, J. R., and E. A. Celarier, Earth surface reflectivity climatology at 340 nm to 380 nm from TOMS data. *J. Geophys. Res.*, 102, 28,003-28,011, <https://doi.org/10.1029/97JD02074>, 1997.
- Herman, J. R., E. Celarier, and D. Larko, UV 380 nm Reflectivity of the Earth's Surface, Clouds, and Aerosols. *J. Geophys. Res.*, 106, 5335-5351, <https://doi.org/10.1029/2000JD900584>, 2001.
- Herman, J., Huang, L., McPeters, R., Ziemke, J., Cede, A., and Blank, K.: Synoptic ozone, cloud reflectivity, and erythemal irradiance from sunrise to sunset for the whole earth as viewed by the DSCOVR spacecraft from the earth-sun Lagrange 1 orbit, *Atmos. Meas. Tech.*, 11, 177-194, <https://doi.org/10.5194/amt-11-177-2018>, 2018.
- Jaross, G., Chen, G., Kowitt, M., Warner, J., Xu, P., Kelly, T., Linda, M., Flittner, DF., 2012, Suomi NPP OMPs limb profiler initial sensor performance assessment. *Proceedings of the SPIE*, Volume 8528, article id. 852805, doi:10.1117/12.979627, 2012.
- Krotkov, N. A., P. K. Bhartia, J. R. Herman, V. Fioletov, and J. Kerr, Satellite estimation of spectral surface UV irradiance in the presence of tropospheric aerosols 1: Cloud free case. *J. Geophys. Res.*, 103, 8779-8793, <https://doi.org/10.1029/98JD00233>, 1998.
- Krotkov, N. A., J. R. Herman, P. K. Bhartia, Z. Ahmad, V. Fioletov, Satellite estimation of spectral surface UV irradiance 2: Effect of horizontally homogeneous clouds. *J. Geophys. Res.*, 106, 11743-11,759, <https://doi.org/10.1029/2000JD900721>, 2001.
- Marshak, A., J. Herman, A. Szabo, K. Blank, A. Cede, S. Carn, I. Geogdzhayev, D. Huang, L. Huang, Y. Knyazikhin, M. Kowalewski, N. Krotkov, A. Lyapustin, R. McPeters, O. Torres, and Y. Yang, 2018: Earth Observations from AMERICAN METEOROLOGICAL SOCIETY DSCOVR/EPIC Instrument. *Bull. Amer. Meteor. Soc.* doi:10.1175/BAMS-D-17-0223.1, 2018.
- Marshak Alexander, Delgado-Bonal Alfonso, Knyazikhin Yuri, Effect of Scattering Angle on Earth Reflectance, *Front. Remote Sens.*, 2, DOI=10.3389/frsen.2021.719610, 2021.
- McPeters, R., Frith, S., Kramarova, N., Ziemke, J., and Labow, G.: Trend quality ozone from NPP OMPs: the version 2 processing, *Atmos. Meas. Tech.*, 12, 977–985, <https://doi.org/10.5194/amt-12-977-2019>, 2019.



318 Penttilä, Antti, Karri Muinonen, Olli Ihalainen, Elizaveta Uvarova, Mikko Vuori, Guanglang Xu, Jyri
319 Näränen, Olli Wilkman, Jouni Peltoniemi, Maria Gritsevich, Heikki Järvinen, Alexander Marshak, Earth's
320 albedo time series reveals low radiative energy input in December 2020, Nature Portfolio,
321 DOI:10.21203/rs.3.rs-677927/v1, 2021.
322
323
324 Thuillier, G., M. Hersé, D. Labs, T. Foujols, W. Peetermans, D. Gillotay, P. C. Simon and H. Mandel, The
325 solar spectral irradiance from 200 to 2400 nm as measured by the Solspec spectrometer from the Atlas
326 and Eureka missions, Solar Physics 214: 1–22, 2003.
327



Figure Captions

329

330 Fig.1 Panel A: Percent reflected solar energy PSE for the Earth from 90°S to 90°N in the narrow band
 331 388 ± 1.5 nm (black circles one for each EPIC scene) from clouds, aerosols, and surface as a function of
 332 time and SEV angle (orange curve – right axis). There are about 6000 points per year. Panel B: 2-week
 333 running average to more clearly show the December and June peaks.

334

335 Fig. 2 EPIC's daily variation of $P(t)$ caused by the Earth's rotation for $\Delta\theta = 90^\circ\text{S}$ to 90°N from 20 March
 336 2016 to 30 March 2016 corresponding to the grey circles in Figure 1A. The numbers 20 to 30 represent
 337 the dates in March 2016.

338

339 Fig. 3 The ratio $R_A = A(2020)/\langle A(2015-2018) \rangle$ of the Earth's area within the specified latitude
 340 bands seen by EPIC in 2020 to that seen during the years 2015-2019. In December 2020, the ratio is 1.03
 341 for 35°S , 55°S , and 65°S , and 1.04 for 45°S . The red curve is Loess(2-months). The inset in 70°S - 60°S
 342 shows the details near December 2020.

343

344 Fig. 4 EPIC SH percent reflected solar energy in the $P_{SE}(388 \pm 1.5$ nm) band (grey circles), the SEV angles
 345 (orange). Magnified details are shown in the Appendix Fig. A1.

346

347 Fig. 5 Monthly average of SH annual time series of percent reflected energy at 388 ± 1.5 nm for 5 years,
 348 2015 – 2021 for 4 latitude bands.

349

350 Fig. 6 One-week least squares running averages Loess(0.035) of P_{SE} values from Fig. 3 as a function of
 351 latitude for the periods Dec 2020 ($SEV = 1.95^\circ$) and November 2021 ($SEV = 2.53^\circ$) compared to the
 352 average of the preceding 4 years, 2015-2018 ($4^\circ < SEV < 6^\circ$). The symbols $\langle A-B \rangle$ denote average. The
 353 inset shows the percent difference P_D as defined in Eq. 10.

354

355 Fig. 7. A time series of OMPS-NM hemispheric zonal average P_{SE} (1 point per day grey circles) 2015-
 356 2021.5 and a 1-week average (red curve) for the band 40°S to 50°S compared to EPIC P_{SE} . The red-curve
 357 is a 1-week running average Loess(0.028).

358 Fig. 8 EPIC NH percent reflected solar energy in the $P_{SE}(388 \pm 1.5$ nm) band (grey circles), the SEV angles
 359 (orange). Magnified details are shown in the Appendix Fig. A1.

360

361 Fig. 9 The ratio $R_A = A(2020)/\langle A(2015-2018) \rangle$ of the Earth's area within the specified latitude bands
 362 seen by EPIC in 2020 to that seen during the years 2015-2019. In June 2020, the ratio is 0.96 for 35°N ,
 363 0.96 for 45°N , 0.97 for 55°N , 0.93 for 65°N . The red curve is Loess(2-months).

364

365 Fig. 10 Peak 1-week least squares running averages Loess(0.006) of P_{SE} values from Fig. 8 as a function
 366 of latitude for the periods June 2020 ($SEV = 2.46^\circ$) and June 2021 ($SEV = 1.83^\circ$) compared to the average
 367 of the preceding 4 years, 2016-2019 ($4^\circ < SEV < 6^\circ$). The symbols $\langle A-B \rangle$ denote average. Inset is Percent
 368 Difference P_D vs Latitude as in Eq. 10.



369 Fig. 11 Monthly average of NH annual time series of percent reflected energy at 388 ± 1.5 nm for 4 years,
370 2015 – 2021.

371

372

373

374